Marine Pollution Bulletin 193 (2023) 115259

Contents lists available at ScienceDirect

Marine Pollution Bulletin

journal homepage: www.elsevier.com/locate/marpolbul

Numerical investigation of the three-dimensional paths of plastic polymers in the Gulf of Naples

Luigi Gifuni [a,*], Paola de Ruggiero [a], Daniela Cianelli [b,c], Stefano Pierini [a,c], Enrico Zambianchi [a,c]

[a] Department of Science and Technologies (DiSt), Parthenope University of Naples, 80143 Naples, Italy
[b] Department of Research Infrastructures for Marine Biological Resources, Stazione Zoologica di Napoli Anton Dohrn, Villa Comunale, 80121 Naples, Italy
[c] CoNISMa (National Inter-University Consortium for Marine Sciences), Piazzale Flaminio, 00196 Rome, Italy

ARTICLE INFO

Keywords:
Tyrrhenian Sea
Gulf of Naples
Marine debris
Three-dimensional paths
Lagrangian simulation

ABSTRACT

The high-resolution Campania Regional Ocean Model (CROM), coupled with an online Lagrangian particle tracking algorithm, is used to investigate the horizontal and vertical behavior of different (in terms of size and density) plastic polymer types during February and August 2016 in the Gulf of Naples. The transport of passive particles is evaluated based on the three-dimensional Eulerian velocity fields provided by the ocean model. The virtual particles are released in several hot spot areas in the Gulf of Naples where most of the marine debris is supposed to come from. A sensitivity analysis on the vertical sinking for negatively buoyant particles is carried out. The sinking behavior is determined by the settling velocity, which depends on the physical properties of the individual litter item as well as on the hydrodynamical features of the marine environment. Different numerical experiments are carried out to evaluate the effect of marine dynamics on three-dimensional transport.

1. Introduction

Plastic debris is currently the most abundant type of litter in the ocean (Derraik, 2002; Topçu and Oztürk, 2010; Fossi et al., 2020; Erni-Cassola et al., 2019; van Sebille et al., 2020). According to the International Union for Conservation of Nature (IUCN), the main sources of plastic debris found in the ocean are land-based, coming from urban and stormwater runoff, inadequate waste management, and industrial activities (Cooper and Corcoran, 2010; Schmidt et al., 2017; Zambianchi et al., 2017). Ocean-based plastic pollution originates primarily from the fishing industry, nautical activities, and aquaculture (Derraik, 2002; Thushari and Senevirathna, 2020; Galgani et al., 2015).

Once they reach the marine environment, the fate of plastic particles will depend on several factors: their nature (size, density, and shape) will determine either their sinking (and therefore, probably, their sedimentation on the seabed) or their floating at the sea surface with potential beaching in coastal regions. However, the situation is much more complex than this, since changes in the physical properties, e.g., fragmentation, degradation (Andrady, 2017) or the interaction with biota (Law and Thompson, 2014) as well as turbulent and chaotic sea motions, can greatly influence plastic particles transport, thus limiting our ability to predict it.

This study aims to analyze the horizontal and vertical transport of different plastic polymer types for two reference months, February and August 2016, in a coastal area of the Tyrrhenian Sea, Western Mediterranean, the Gulf of Naples (GoN), during which model data are available. The choice of a winter (February 2016) and a summer month (August 2016) in our simulations aims to understand how seasonality, and thus the different hydrological features of the marine environment, affect the 3D transport of plastic particles.

Due to the presence of numerous tourist attractions, the high population density, and the intense maritime commercial activity, the GoN is strongly affected by marine pollution, thus its coastal waters present hydrographic and biological properties reflecting anthropic stress (Ribera d'Alcala et al., 1989; Zingone et al., 2010; Cianelli et al., 2012; Castagno et al., 2020). A study by Angiolillo et al. (2015) shows that deep marine layers are also heavily polluted, debunking the common idea that these areas are less impacted by anthropogenic activities (Hinderstein et al., 2010). Thanks to the use of ROVs equipped with digital cameras, the main pollutants of the seabed in Campania, Sicily, and Sardinia were analyzed (Angiolillo et al., 2015). The study shows that the highest median value of debris abundance was found in

* Corresponding author.
E-mail address: luigi.gifuni1@studenti.uniparthenope.it (L. Gifuni).

https://doi.org/10.1016/j.marpolbul.2023.115259
Received 9 March 2023; Received in revised form 1 July 2023; Accepted 3 July 2023
Available online 7 July 2023

Campania while the lowest value was recorded in Sardinia, emphasizing the relationship of debris abundance with the average human population density in the analyzed regions (429, 196, 68 habitants per km^2, for Campania, Sicily, and Sardinia, respectively). Regarding the class of pollutants, the study shows that fishing gears were the dominant source of debris (89 %) while plastic and other debris were occasionally found, representing respectively 5 % and 6 % of the samples. However, the data from Angiolillo et al. (2015) indicate that the evidence of this type of debris can be biased on the kind of explored sea bottom and the employed methods (Watters et al., 2010). For this reason, observation surveys and monitoring networks in coastal areas should be increased.

The use of an ocean model coupled with a Lagrangian particle tracking algorithm allows us to fill the observational gap and define scenarios to test possible pathways, main sources, and potential accumulation zones of plastic debris (van Sebille et al., 2020; Zambianchi et al., 2014). Observations allow us to set the stage for our simulations (e.g., defining release areas, choice of pollutant type, concentration, etc.) to produce targeted analyses.

Here, we use the high-resolution Campania Regional Ocean Model (CROM, de Ruggiero et al., 2016), coupled with an online Lagrangian particle tracking algorithm. The virtual particles are released in several hot spot areas in the GoN, where most of the marine debris is supposed to come from, and a sensitivity analysis on the vertical sinking for negatively buoyant particles is carried out.

We organized our study as follows: in Section 2 the CROM, the adopted particle-tracking algorithm, and the numerical simulation setup (description of the chosen type of polymers and definition of the release area) are discussed. In Section 3 the numerical simulation results are provided. Finally, conclusions are drawn in Section 4.

2. Model and methods

2.1. The circulation model

The CROM (de Ruggiero et al., 2016) is implemented on a domain that includes the Campania Coastal System (CCS, see Fig. 1a) with a horizontal spatial resolution of 1/144° (Δy ≈ 772 m, Δx ≈ 579–591 m). It is based on the Princeton Ocean Model (POM, Blumberg and Mellor, 1987; http://www.ccpo.odu.edu/POMWEB/) and is one-way nested with the NEMO-OPA (Nucleus for European Modeling of the Ocean-Ocean Parallelise, Madec, 2008) implemented over the whole Mediterranean Sea with a 1/16°-horizontal resolution and 71 vertical layers (see Oddo et al., 2009 for model configuration). The POM adopts the mode splitting technique; here the time step for the external (internal) mode is $\Delta t = 1s$ ($\Delta t = 60s$) (as in de Ruggiero et al., 2016).

The momentum, heat, freshwater, and radiative fluxes are computed by bulk formulas with atmospheric parameters provided by the non-hydrostatic SKIRON/Eta atmospheric modeling system (http://forecast.uoa.gr/forecastnewinfo.php) of the National and Kapodistrian University of Athens with 5 km-horizontal resolution. The nesting technique and the bulk formulas used are described in detail in de Ruggiero et al. (2016). Twelve monthly hindcasts referring to the year 2016 are produced (de Ruggiero et al., 2020; Gifuni et al., 2022).

2.2. Particle-tracking model

The 3-dimensional particle trajectories are computed by the subroutine TRACE of the Princeton Ocean Model and integrated with vertical settling velocity; for a description of the algorithm see Berntsen et al. (1994). The particles motion is described by Lagrangian equations:

$$\frac{dx_p}{dt} = u(x_p, y_p, z_p) \tag{1}$$

$$\frac{dy_p}{dt} = v(x_p, y_p, z_p) \tag{2}$$

$$\frac{dz_p}{dt} = w(x_p, y_p, z_p) \tag{3}$$

where (x_p, y_p, z_p) is the 3-dimensional position of the particle, and (u,v,w) is the 3-dimensional velocity Eulerian current velocity field provided by CROM. The algorithm applies a bilinear spatial interpolation to obtain the current field in particle position and a linear interpolation in time to obtain the velocity values at any Lagrangian timestep. The vertical coordinates z_p are transformed into the sigma coordinates (σ) of the Eulerian model before the tracer particles are propagated, and after propagation, they are transformed back to z_p. The vertical transformations are computed with this expression:

$$\sigma = \frac{z_p - \eta}{H + \eta} \tag{4}$$

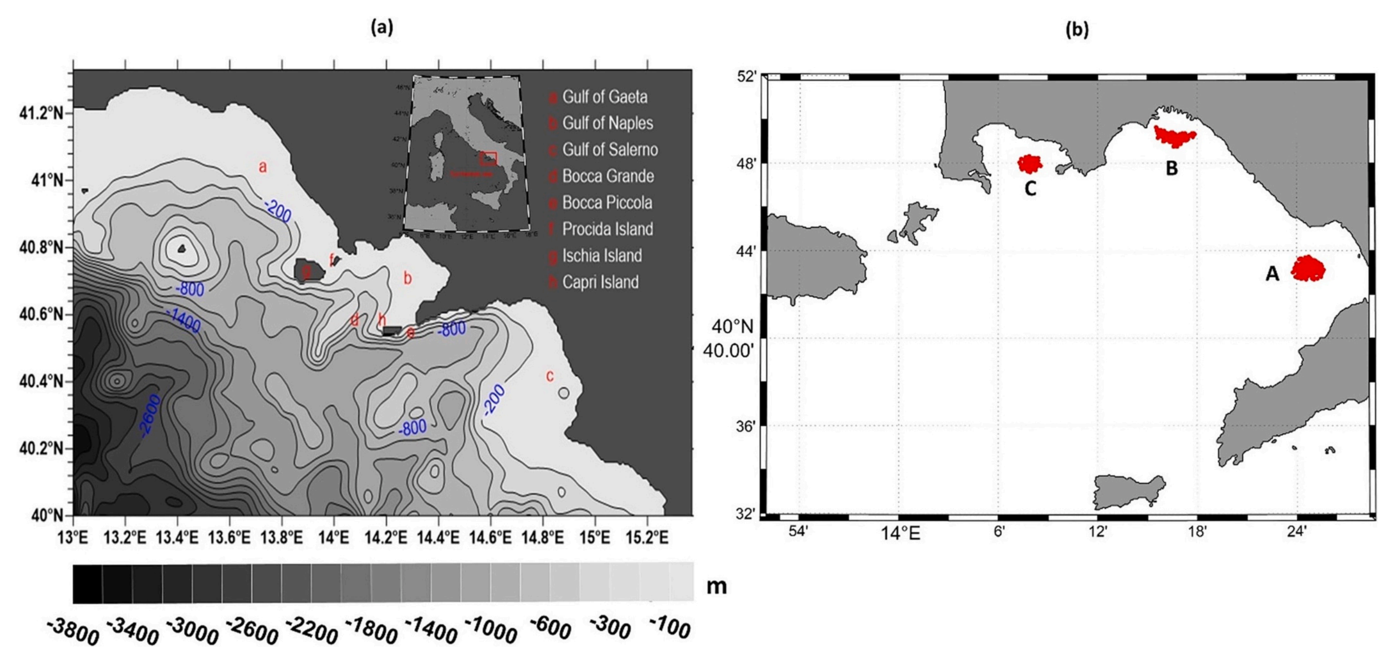

Fig. 1. (a) CROM Domain of integration and bathymetry. (b) A, B, and C are the particles release points of our numerical investigations in the GoN.

where σ is the vertical coordinate of the 3-dimensional current field calculated by the CROM, H is the bathymetry of the CROM domain and η is a free surface simulated by the CROM.

Eqs. (1)–(3) are solved with a first-order forward Euler scheme (in the current implementation of TRACE, it is not possible to choose a high-order numerical scheme).

The coupling of CROM with a more advanced Lagrangian particle tracking algorithm and the validation of the numerical results will be the subject of future works.

Particles are prevented from crossing the bottom or free surface, as well as horizontal boundaries, as adopted by Beletsky et al. (2006) and Beletsky et al. (2007).

We have incorporated in the subroutine TRACE a settling velocity (*ws)* as a function of the size and density of the particle with the formula suggested by Zhiyao et al. (2008) which applies to all *particle Reynolds numbers* (R_e, see Zhiyao et al., 2008; de Leo et al., 2021; de la Fuente et al., 2021) $<2 \times 10^5$ defined according to Eq. (5):

$$R_e = \frac{4d_*^3}{3A} \tag{5}$$

$$w_s = \frac{\nu}{2R} d_*^3 \left[\left(\frac{3A}{4} \right)^{2/n} + \left(\frac{3B}{4} d_*^3 \right)^{1/n} \right]^{-n/2} \tag{6}$$

where the coefficients A and B are evaluated by Zhiyao et al. (2008) using a trial-and-error procedure to minimize the error-predicted data computed with Eq. (6) and several experimental data provided by Engelund and Hansen (1967) and Cheng (1997). This leads to A = 32.2; B = 1.17 and n = 1.75 and to Eq. (7) adopted in our numerical simulation:

$$W_S = \frac{\nu}{2R} d_*^3 \left(38.1 + 0.93 d_*^{\frac{12}{7}} \right)^{-\frac{7}{8}} \tag{7}$$

where ν is the kinematic viscosity coefficient of seawater (1.15×10^{-6} m^2/s), R is the radius of the spherical particle, and d_* is the dimensionless diameter of the particle estimated as:

$$d_* = 2R \left(g \left(\rho_p - \rho_w \right) / \rho_w \nu^2 \right)^{1/3} \tag{8}$$

where g is the gravity, ρ_p is particle density and ρ_w is the seawater density.

Finally, in the present study, we model marine plastics motions as Lagrangian transport with vertical settling. In the horizontal, plastics travel with the simulated horizontal ocean currents i.e., they are passively advected by the flow. In the vertical, their motion is driven by 2 components: (i) w, the vertical component of the Eulerian current field provided by the CROM, and (ii) *ws*, the local settling velocity of the plastic material (Zhiyao et al., 2008). An implicit assumption is thus of quasi-staticity, i.e., the material is assumed to reach the settling velocity immediately (Lermusiaux and Coauthors, 2019). Thus, the total vertical velocity (w_{tot}) governing the displacement of particles in the water column is the algebraic sum of w and *ws*. We recall that CROM determines w from the continuity equation using the horizontal velocity and surface elevation (Blumberg and Mellor, 1987).

To detect the influence of w on the vertical dynamics of the plastic materials and the final fate of the trajectories, we performed a sensitivity analysis by comparing the results obtained by taking into account w in the computation of w_{tot} with the ones obtained by neglecting it.

Here we emphasize that, once a particle reaches the seabed (settling) or a cell adjacent to a coastal cell (beaching), that is, in those locations without velocity data, it remains fixed at its last valid position for the residual run period.

2.3. Configuration of numerical simulations

We performed a 3D numerical simulation (3DS) referred to February and August 2016 using the CROM coupled with TRACE integrated with the vertical settling velocity provided by Zhiyao et al. (2008).

As pointed out by de la Fuente et al. (2021) the variation of the seawater density also plays a critical role in the particle settling dynamics. As particles move in the ocean, they experience different values of the ambient fluid density, which could increase or decrease the settling rate. So, the choice of a winter month (February 2016) and summer month (August 2016) in our simulations aims to understand how seasonality, and thus the very different vertical stratification, affect the 3D transport of plastic particles. As to the release area, we have identified 3 hotspot (HS) areas (Fig. 1b) from which we assume that the largest marine plastic debris spills come: the Sarno River mouth, the harbor of Naples, and the coastal area of Bagnoli.

This choice is consistent with the study of Tornero and Ribera d'Alcalà (2014), in which they analyze the metal contamination in the Campania region. The Sarno River estuary (point A in Fig. 1b) is strongly affected by several pollution sources and is one of the main contributors to metal loads into the GoN and the Tyrrhenian Sea. In the harbor of Naples (point B in Fig. 1b), all the chemical elements considered in the study (such as Pb, Zn and Hg) exceed the Italian legal thresholds. Most of the metal pollution in the area is anthropogenic and linked to the different industrial and commercial activities of the harbor. Concentrations of metals tend to diminish as one moves away from this area, reaching levels close to the background near the bay entrance (Baldi et al., 1983; Griggs and Johnson, 1978; SiDiMar, 2005). As to the coastal area of Bagnoli (point C in Fig. 1b), despite industrial activities being all shut down between 1990 and 2000, the elevated chemical concentrations are suggestive of an active source of contamination (Albanese et al., 2010). Therefore, although Tornero and Ribera d'Alcalà (2014) do not refer directly to plastic waste pollution, it is evident that the defined areas suffer particularly from the influence of anthropogenic activities, thus we can assume them as our HSs.

Once the release areas were defined, the type and size of the plastic particles had to be chosen. Here we wanted to focus on negatively buoyant rigid polymer classes, with a density greater than the nominal density of the seawater equal to 1025 kg/m^3. In detail, based on the density classification of different polymer types reported in Horton and Dixon (2018) three transport case studies were carried out: one involved Polystyrene (PS – with a density of 1050 kg/m^3); one Polyamides (PA – with a density of 1130 kg/m^3); the last one Polyethylene terephthalate (PET – with a density of 1350 kg/m^3). Moreover, a sensitivity study was carried out to evaluate the influence of w on the particle trajectory. Table 1 also shows the common uses of these plastic types.

Once the polymer types were defined, we needed to evaluate the maximum particle size for which *ws* (Eq. (7)) was verified. As previously described, *ws* is valid for $R_e < 2 \times 10^5$ (Eq. (5)) and this range of applicability imposes some constraints on the choice of particle size. Fig. 2 shows the evolution of R_e as a function of the size (diameter) and density of the particle. It should be noted how R_e (black line in Fig. 2) increases with the increase of the diameter length and density of the chosen polymer types. The horizontal red dashed line ($Re = 2 \times 10^5$) and the vertical red dashed line (max. Diameter size) in the figure highlights the

Table 1
Polymer types and their common use.

Polymer type	Common use
Polystyrene (PS)	Food containers, plastic tableware, disposable cups, plates, cutlery, CDs, and audio tape boxes.
Polyamides (PA) (Nylons)	Fibers, toothbrush bristles, fishing lines, wear pads, wheels, gloves, electrical connectors, and tennis racket strings.
Polyethylene terephthalate (PET)	Carbonated drinks bottles, peanut butter jars, plastic film, microwavable packaging, plastic bottles

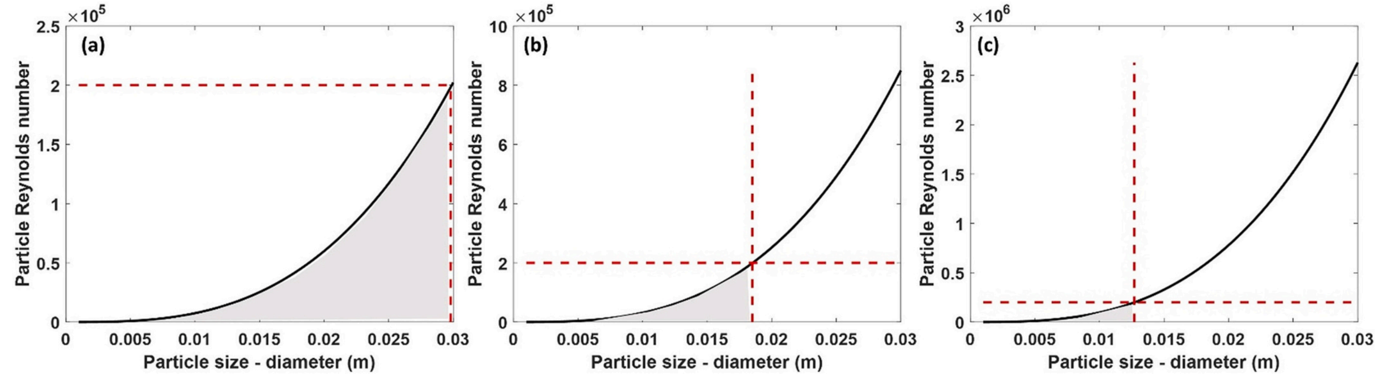

Fig. 2. Particle Reynolds number increment for (a) 1050 kg/m3 (PS), (b) 1130 kg/m3 (PA) and (c) 1350 kg/m3 (PET) particle density. The shadow area defined from the horizontal and vertical red dashed lines marks the range of applicability of the settling velocity equation. (For interpretation of the references to colour in this figure legend, the reader is referred to the web version of this article.)

applicability range (shaded area in Fig. 2) of Eq. (7). Table 2 also shows the maximum particle diameter size, as a function of the polymer density (PS in Fig. 2a, PA in Fig. 2b, PET in Fig. 2c), that we can adopt in our simulation to ensure the validity of Eq. (7). However, if we chose a particle diameter size equal to half of the maximum diameter (so that the constraint defined by Eq. (7) is respected), we would obtain the settling rates given in Table 3. Moreover, if we considered the depth of the seabed in HS areas (about 60 m), the particles would reach the bottom very quickly and would not be affected by the horizontal transport contribution.

To reproduce slowly sinking plastic particles, with the density defined by the chosen polymer types, it is necessary to reduce the particle diameter size, thus falling within the microplastics (MPs thereafter) category (< 5 mm; Rocha-Santos and Duarte, 2015). We chose a radius of 0.03 mm in such a way that it was possible to evaluate both the contribution due to horizontal transport and the variation in the settling velocity due to changes in seawater density. The number of particles involved in the simulations was 500 for each HS area, released at the beginning of each month. Since particles were completely immersed in the water column, the windage effect was not considered.

Typically, different Lagrangian transport algorithms include a random walk component to take into account the sub-grid scale turbulent particle motion both in the horizontal and vertical direction (de la Fuente et al., 2021; Jalón-Rojas et al., 2019; Liubartseva et al., 2018). However, in our simulation, the turbulent nature of the flow was neglected. We refer the reader to Cianelli et al. (2013) where a sensitivity study is done to identify the weight of the diffusive component in the transport of passive tracers within the GoN. In the work, in addition to advection by surface currents and wind drift, a stochastic component to particle motion, in the form of a random walk (e.g., Csanady, 1980) parameterized by eddy diffusivity, was also included. The analysis shows that in most of the analyzed scenarios, the diffusive component does not lead to meaningful differences in the results, proving that the advective component is the main driver of the transport processes in the GoN. However, although this is particularly true in the case of relatively stable dynamic regimes or strong current fields, in weak or null wind conditions, the diffusive component starts to become important, influencing e.g., the residence times of the passive tracers released in the area.

Table 2
Maximum particle diameter for which the settling velocity equation was verified.

Density (kg/m^3)	Max. diameter size (m)
1050	0.0298
1130	0.0185
1350	0.0127

Table 3
Sinking rates as a function of polymer types for half the maximum diameter size.

Polymer type	Radius (m)	Settling velocity (m/min)
PS	0.007	3.6
PA	0.0045	5.4
PET	0.003	8.4

A sensitivity study will be carried out in future works to assess how different parameterizations of the diffusive (both horizontal and vertical) processes affect the 3D fate of passive tracers. The implementation of this component will enable us to provide more realistic simulations. Limitations of the model are acknowledged in Section 4.

We adopted the same configuration (as to the particle number and distribution, and as to the size and type) for both February and August simulations. Following Duran et al. (2018), the computational time step was chosen to satisfy the CFL condition.

$$\Delta t < C\frac{\sqrt{\Delta x^2 + \Delta y^2}}{c} \tag{9}$$

where c is the maximum velocity simulated by CROM in the investigation period and $C = O(1)$ is the dimensionless Courant number (here assumed to be equal to unity). As Duran pointed out, if the CFL condition is not satisfied one tracer particle could overshoot through one or more grid cells without taking into account the information within the grid cell (such for example the fluid velocity). In this case, the resulting trajectory would be spurious and therefore not error-free. We set $\Delta t =$ 10' as the results from the CROM grid resolution ($\Delta x \approx 579 - 591\ m$, $\Delta y \approx 772\ m$) and maximum velocity (c) of $\approx 0.57\ m/s$. Moreover, we tested the sensitivity of our results using several lower Lagrangian integration time steps (not provided). We found that going below this sampling time (10′) does not bring any advantage in the tracer trajectory but, on the other hand, highly increases the computational cost (especially in our case, in which all the CROM simulated three-dimensional fields are involved to properly compute the particle trajectories).

We would like to emphasize that, considering the uncertainties resulting from the lack of observed data in the area (both in the input sources and the nature of the pollutants) our purpose is to provide a first attempt to study the three-dimensional dispersion of negatively buoyant plastic polymers and how the different hydrodynamical conditions of the two test periods affect their vertical and horizontal dynamics. Thus, we aim to assess the importance of sub-surface advection for the transport pathways of marine debris and lay the basis for future works that will also help the interpretation of measurements.

3. Results and discussion

3.1. Dynamical conditions and reconstructed trajectories

Here we analyze the different transport scenarios, according to the configuration described in the previous section (2.3), regarding February and August 2016. An initial assessment of the different results obtained by considering (or neglecting) the effect of *w* in the numerical configuration will also be analyzed. We will therefore indicate with PSV-PAV-PETV the three scenarios obtained by considering *w* in the vertical dynamics ($w_{tot} = w + ws$, for PS, PA, and PET respectively); with PSN-PAN-PETN the scenarios obtained by neglecting it (in other words, the vertical dynamics will be driven by *ws* alone).

First of all, we will briefly describe the monthly mean-basin scale circulation pattern for the analyzed period (readers should refer to de Ruggiero et al., 2020 for more detail about the hydrodynamical model results).

Fig. 3a-b-c (Fig. 3d-e-f concern the summer scenario) show the monthly mean current at the surface (Fig. 3a-d), at 50 m depth (Fig. 3b-e) and at 100 m depth (Fig. 3c-f) superimposed on the magnitude of the current field. With regards to the winter periods and focusing on the surface layer (Fig. 3a), it should be noted how the northward Tyrrhenian current leads the sea surface waters through the "Bocca Piccola" (the passage between Capri and the Sorrento peninsula) and the "Bocca Grande" (the main passage of the gulf between Ischia and Capri islands) straits. Overall, the sea surface current is directed towards the coast. At 50 m and 100 m depth (Fig. 3b e 3c), we observe a rotation of the current field, with an offshore current near the coastline. While in winter the Tyrrhenian current off the "Bocca Grande" opening is mainly directed northwards (see Fig. 3a), in August it is directed southwards (Fig. 3d), allowing the Tyrrhenian Sea water to enter through the Ischia and Procida channels and exit through the "Bocca Piccola" straits. In addition, while a surface cyclonic structure drives the water masses inside the GoN (Fig. 3d), a reverse flow is observed at 50 and 100 m depth (Fig. 3e and f). MP particle trajectories will evolve under these dynamical conditions.

Let us now analyze the PSV, PAV, and PETV simulated results. Fig. 4a (4b) show the fate of the trajectories of PS, PA, and PET spherical particles for the winter (summer) period. In this case, *w* also plays a role in the vertical dynamics. In winter, based on the analysis of the average trajectories (not provided), we saw that the particles are originally driven by an inshore current field, in all the release areas. During the sinking, the offshore current carries them far from the coastline. Regarding the summer scenarios, the sub-surface anticyclonic structure affects the PS particle's evolution paths. In B (see Fig. 1), the particles are horizontally driven by a south-easterly coastal current which displaces them along the shoreline. This is also the case of the Sarno River mouth (A, see Fig. 1b), where the south-westerly sub-surface current displaces the particles along the shoreline. In C (see Fig. 1), the particles are involved in low horizontal transport and the sinking is almost vertical. In both cases, as the density of the chosen polymer types increases (with fixed radius size), *ws* became stronger with the resulting decrease of the settling time and covered distance. In other words, under these conditions, the settling point will be very close to the release site for polymer types with a higher density like PA (PAV scenario) or PET (PETV scenario). Fig. 4c (4d), on the other hand, provide the endpoint of the MPs particles for those simulations in which the contribution of *w* is neglected (PSN-PAN-PETN) for the winter (summer) periods. From an initial assessment, it should be noted that in the winter case (Fig. 4c) the westward particle advection is reduced compared to the previous scenarios (Fig. 4a). At the same time, in the summer case (Fig. 4d) the horizontal transport of particles is inhibited, resulting in sedimentation that occurs closer to the release site.

3.2. Sensitivity of the microplastics distribution to 3D hydrodynamical conditions

In Section 3.1 we have provided an initial overview of the results obtained for the different scenarios, already highlighting some differences between the summer and the winter case, as well as among the scenarios in which *w* is activated (neglected) in the vertical dynamics. Here we go into the details of the discussion.

Table 4 provides the average distance covered by the particle cluster, derived from Haversine's formula. It is interesting to note that, under the winter conditions, the trajectories reach the largest distances (about 12 km for PS particles) in the harbor of Naples (area B) and the horizontal displacements are greater than the vertical ones according to de la Fuente et al. (2021) and Siegel and Deuser (1997) since the particles are

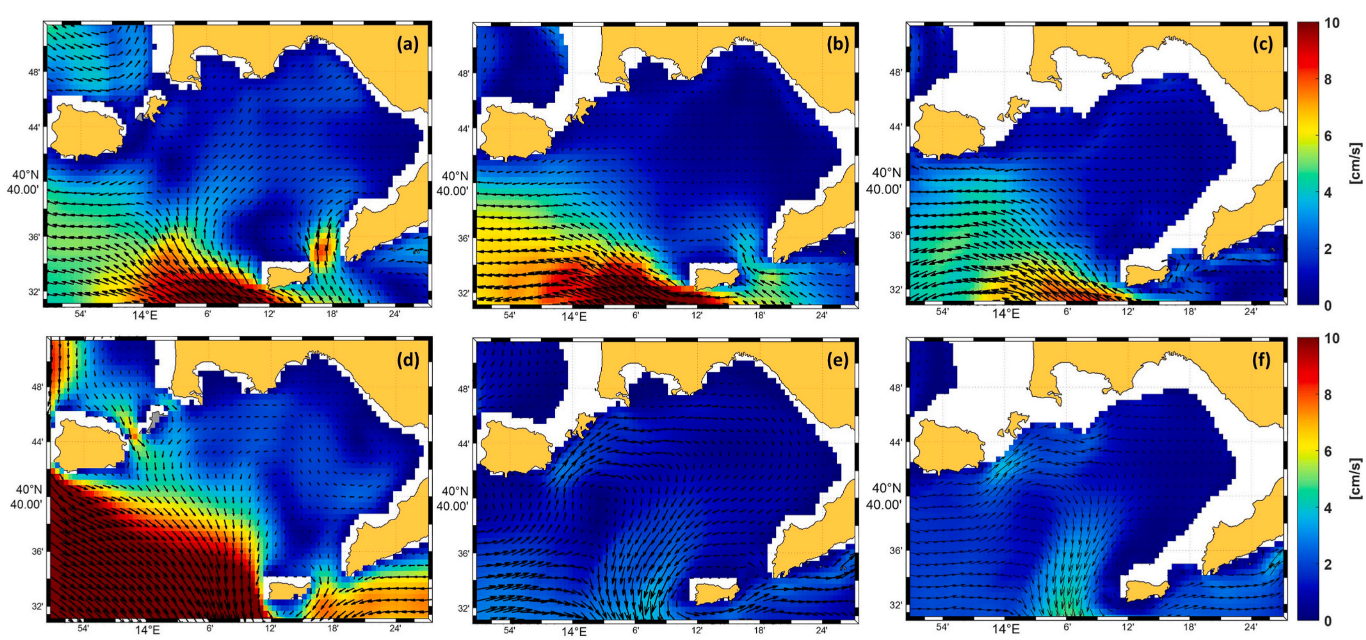

Fig. 3. Monthly mean surface (a-d), 50 m depth (b-e) and 100 m depth (c-f) current fields for February 2016 (a-b-c) and August 2016 (d-e-f). In the background the sea velocity magnitude.

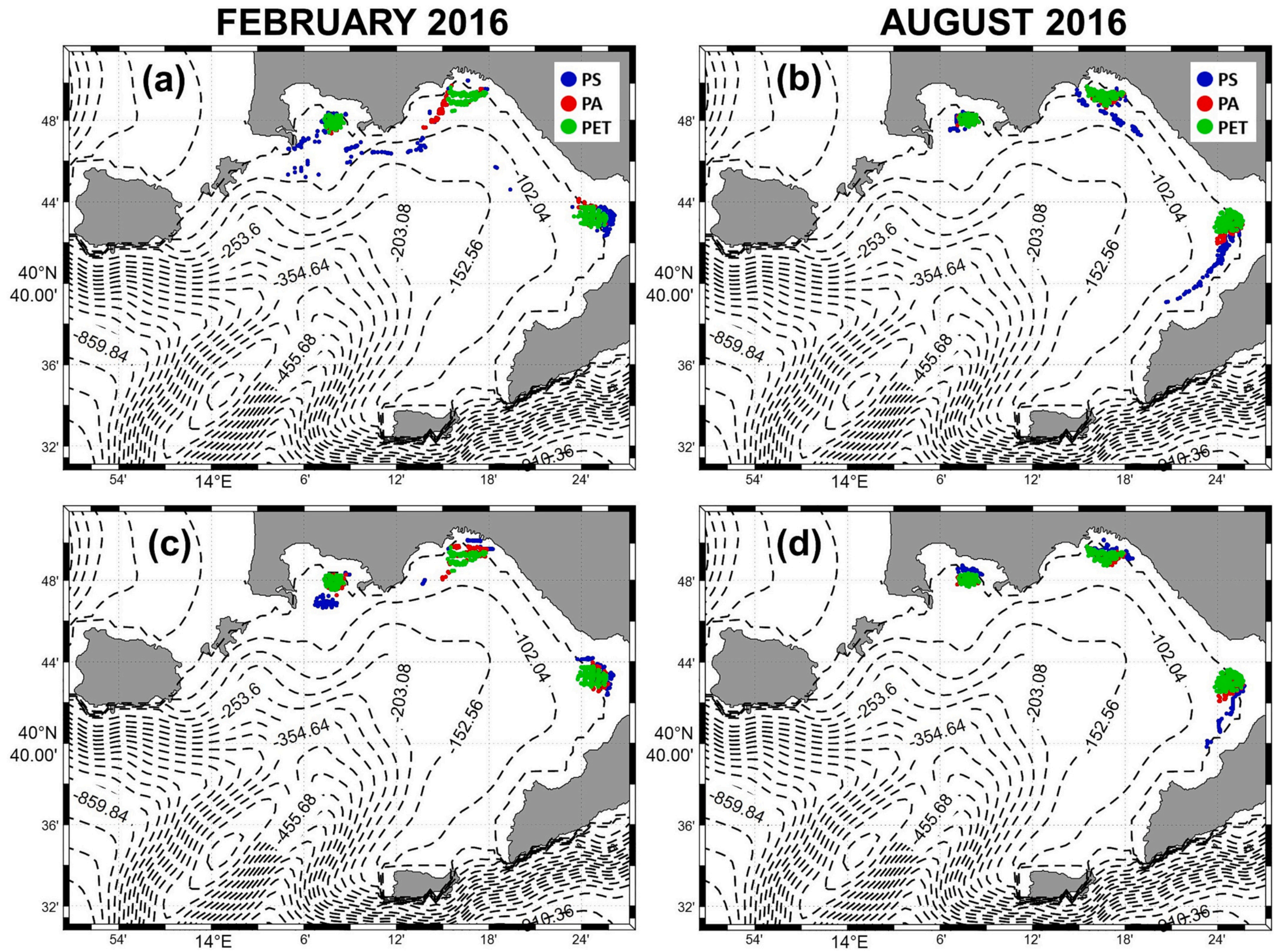

Fig. 4. trajectories for winter (5a-5c) and summer period (5b-5d). Fig. 5c and d shows the trajectories without taking into account w (PSN-PAN-PETN scenarios).

Table 4
Covered distance by the particles for PSV-PAV-PETV scenarios and PSN-PAN-PETN scenarios.

February (distance km)	A	B	C	August (distance km)	A	B	C
PSV	3.32	11.98	6.01	PSV	10.45	5.40	5.01
PAV	3.11	4.69	1.73	PAV	2.02	1.35	1.16
PETV	1.38	1.71	0.80	PETV	0.64	0.59	0.42
PSN	4.41	2.10	5.12	PSN	9.06	4.10	3.43
PAN	2.55	2.73	1.67	PAN	1.83	1.48	1.25
PETN	1.43	1.95	0.83	PETN	0.65	0.61	0.43

sinking sideways. On the other hand, in the summer scenario, in A we observe the largest covered path (about 11 km) as reported in Table 4. Again Table 4 highlights the fact that, as mentioned in Section 3.1, as the density of the chosen polymer types increases, the settling velocity rises with the resulting decrease in the settling time and covered distance.

From the comparison of the two scenarios, an overall decrease in the horizontal distances covered by the particles during the summer case (if we exclude the PSV scenario for the Sarno estuary) should be noted. The reason for this behavior is the following: first, the low-intensity surface and sub-surface current field during the summer period reduces the horizontal transport, thereby enhancing the potential sedimentation in sea areas close to the release zone. In addition, under the dynamical pattern of this investigation period, the particles are displaced not far from the coastline, where the current field is weak. However, the observed evolution at the Sarno estuary for PS polymer types, allows us to highlight the important role of *w* in the vertical particle dynamics. Here, *w* allows the resuspension of several particles by enhancing their lifetime in the water column and therefore their horizontal transport.

Finally, regarding the winter case, for PS (PSN scenario) and PA (PAN scenario), we observe an overall decrease in the traveled distances with the exclusion of the PS particles in the Sarno estuary (4.3 km compared to 3.2 km obtained in the PSV scenario), while for PET (PETN scenario) the distances are approximately the same. Regarding the summer case, the results reported in Table 4 again reflect an overall reduction in the cluster distances (when we neglect *w*) for PSN scenarios while for PAN we observe a slight increase in B and C.

The evolution of the depth reached by the particles in the three release areas is shown in Fig. 5. (Fig. 5a-b-c concern the winter scenarios; Fig. 5d-e-f concern the summer ones). The shaded area shows the range of depths reached by all involved particles, while the solid line shows the mean depth. Here we notice the larger shaded area for the slower sinking particles such as PS (red line in Fig. 5a-b-c), especially in the B area (red line in Fig. 5b), which means high particle displacement. In other words, some particles were advected over greater distances by the mean horizontal and vertical currents, reaching areas where the seabed is deeper. On the other hand, other particles reach a grid cell close to a land cell (in this case the final depth is lower) and will no further be involved in the transport.

To give a more comprehensive overview of the findings, we provide

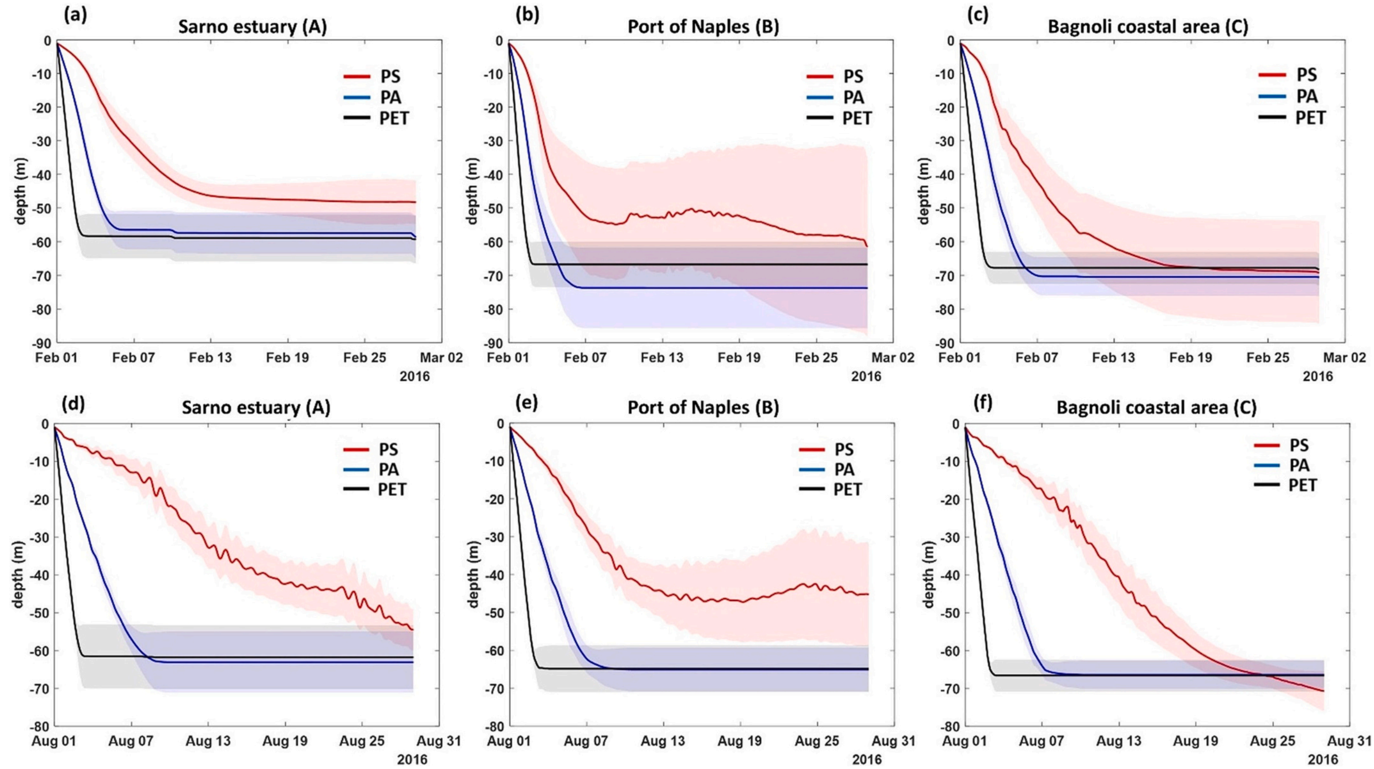

Fig. 5. Evolution of the depth reached by the particles for PSV (red line), PAV (blue line) and PETV (black line) in A (Fig. 5a), B (Fig. 5b), and C (Fig. 5c). The shaded area shows the range of depths reached by all involved particles, while the solid line shows the mean depth. Fig. 5d-5e-5f are the same, but for the summer scenarios. (For interpretation of the references to colour in this figure legend, the reader is referred to the web version of this article.)

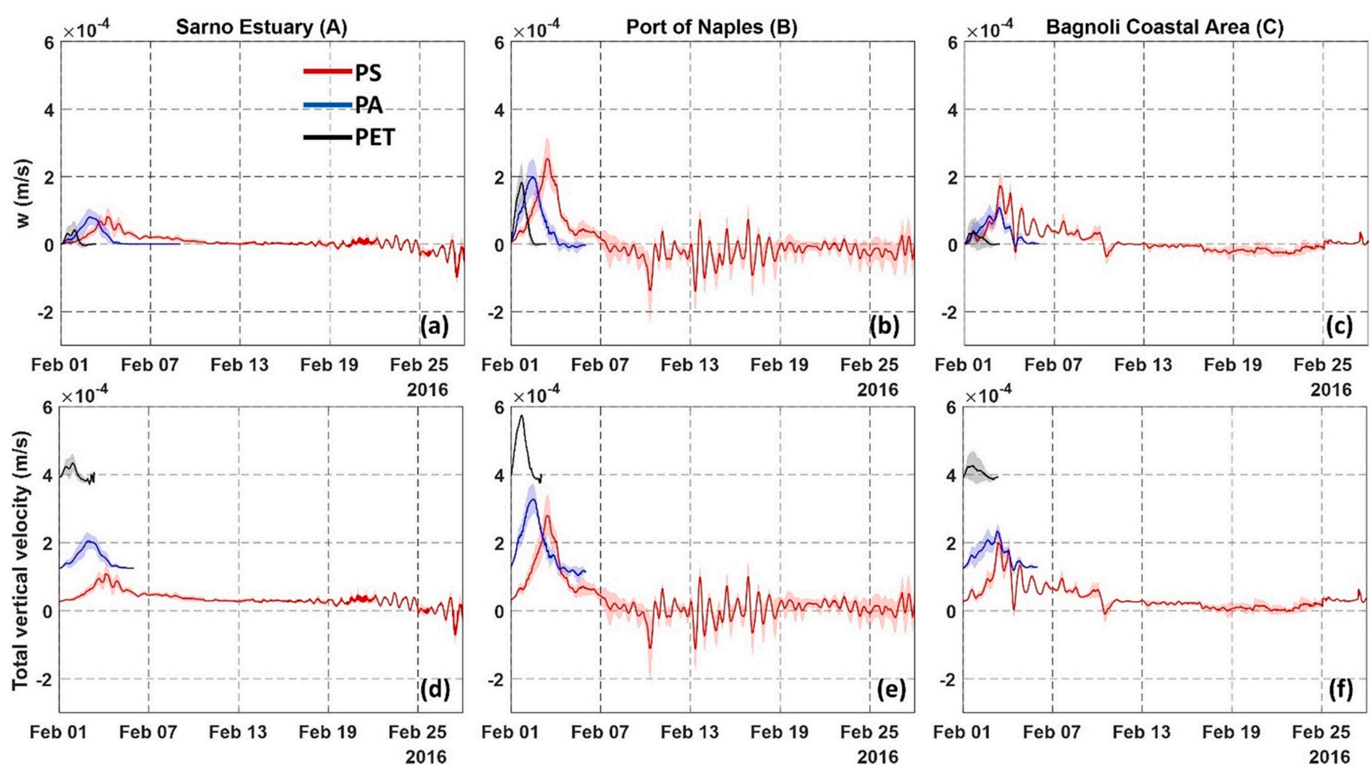

Fig. 6. Timeseries of the sea vertical component (6a-6b-6c) and total vertical velocity (6d-6e-6f) over the paths covered by the particles in February 2016. From left to right the velocity condition in A, B and C respectively (see Fig. 1). For the sake of clarity once all particles have settled, the timeseries ends.

in Fig. 6 both the time series of w (Fig. 6a-b-c) for the three polymer types (red line for PS, blue line for PA, and black line for PET particles) in each HS areas, and the evolution of the w_{tot} (Fig. 6d-e-f) for the winter case. For the sake of clarity, here we assume that positive values of w (w_{tot}) are associated with downward motion (sinking), and, on the other hand, negative ones are associated with upward movement (rising). Moreover, it should be noted that the time series length changes in agreement with the times over which all the involved particles reach the ocean floor. Therefore, longer time series are expected for the less dense PS particles, while shorter ones are expected for particles that sink faster (i.e., PA and PET).

In the simulations involving PA and PET particles, it has been observed that the contribution of the *ws* on the vertical behavior is crucial. The evolution of w_{tot} (Fig. 6d-e-f) clearly shows that *ws* shifts w towards positive values, thus suppressing the horizontal transport and reducing the settling time. Under these conditions, PA particles take an average of 6 days to reach the seafloor, while PET particles take only 2 days (see also Table 4). Meanwhile, although *ws* promotes sinking also for PS particles, its intensity is almost near to w. Therefore, the vertical dynamics of these particles will be mainly driven by the behavior of w.

As done for the winter case, in Fig. 7 we show the average evolution of w (7a-7b-7c) and w_{tot} (7d-7e-7f) over the paths covered by the involved particles (red line for PS, blue line for PA, and black line for PET). Again, it is worth underlying that the time series length changes in agreement with the times over which all the involved particles reach the ocean floor, decreasing as the density of the involved polymers increases. The PS particles, which on average remain within the water column for longer times due to their physical properties, will be greatly affected by w. Moreover, the presence of negative (upward) vertical motions inhibits their settling by enhancing their lifetime in the water column.

In this context, Table 5 provides for the winter (summer) scenario the mean final depth and the residence time (τ_1 and τ_2, see de la Fuente et al., 2021) during which the MPs particles are found in the water column before reaching the seabed. Here, τ_1 is calculated as the ratio between the mean final depth of the seabed reached by the particles and w_{tot} (the sum of *ws* and w), which varies according to the chosen polymer types and the marine dynamics encountered by the particle trajectory, while τ_2 is computed as the ratio between the mean depth and the *ws* (thus we neglect w). The influence of w on the residence times is clear. In winter, for low-density PS particles, when w is involved in the sinking, the associated residence times are reduced ($\tau_1 < \tau_2$). This means that w acts in phase with *ws* (is mainly downward directed) and the sink is fast. The contrary occurs in the summer scenario: in this case, $\tau_1 > \tau_2$, thus w, now dominated by upward-directed (rising) motions, decreases the sinking speed, and consequently, the average residence times are greater. Although the influence is clear for low-density PS particles where we observe a decrease (among the three HS areas) of the average residence time of 7 days (in the winter case) and an increase of 10 days for the summer release, its effect is strongly reduced for PA particles, becoming completely negligible for PET ones. To evaluate areas of flow contraction and expansion where vertical flux could be significant, the monthly mean horizontal divergence at the sea surface (not provided) was calculated. Positive surface divergence is generally indicative of convergence at deeper levels and subsequent upward vertical motion of the sea. On the other hand, regions of negative surface divergence (i.e., convergence) are associated with a downward motion to lower levels.

Table 5
Mean final depth and residence time of the different plastics polymer types. In brackets, the results for the summer scenarios.

PS	Mean final depth (m)	τ_1 (days)	τ_2 (days)
A	48 (57)	17 (29)	21 (24)
B	69 (44)	26 (29)	29 (18)
C	72 (71)	22 (24)	31 (30)
PA			
A	58 (63)	5 (7)	6 (6)
B	75 (65)	5 (6)	7 (6)
C	70 (66)	6 (6)	7 (6)
PET			
A	59 (61)	2 (2)	2 (2)
B	66 (64)	2 (2)	2 (2)
C	68 (66)	2 (2)	2 (2)

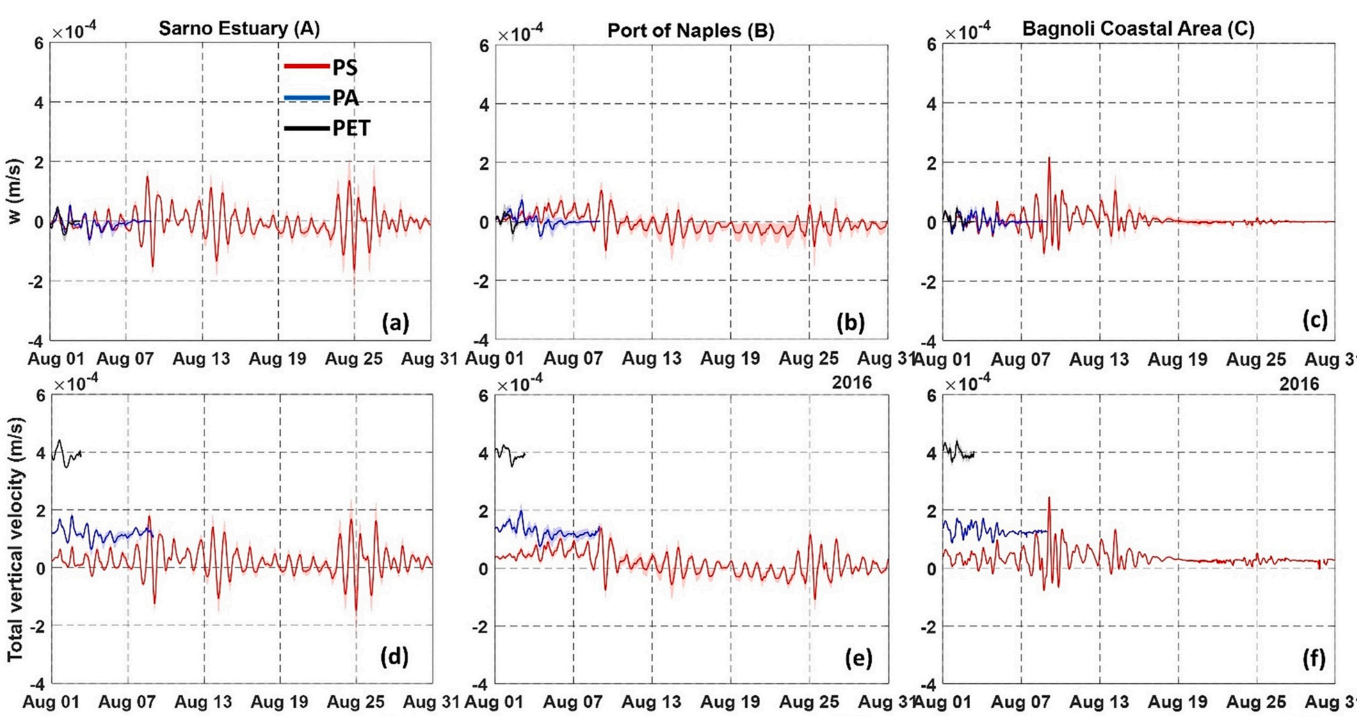

Fig. 7. Timeseries of the sea vertical (7a-7b-7c) and total vertical velocity (7d-7e-7f) over the paths covered by the particles in August 2016. From left to right the velocity condition in A, B and C respectively (see Fig. 1). For the sake of clarity once all particles have settled, the timeseries ends.

Therefore, to unveil localized areas of upward and downward conditions, maps of horizontal divergence were computed. This analysis confirms that in February 2016 there were convergence zones of the flow localized in the HS areas, which are associated with downward motions, leading to an increased sinking and shorter residence times, according to the results provided in Table 4. On the other hand, during August of 2016, a broader positive divergent situation occurred, resulting in an upward vertical component of the sea therefore associated with a decrease in the particles sinking.

Finally, to evaluate the role of seawater density variability on settling velocity, we follow the approach of de la Fuente et al. (2021). Fig. 8a (Fig. 8b, concerning the summer scenario) shows the normalized probability histogram of the seawater density at the positions of the 1500 PS particles at $t = 0$, 15, and 28 days after the release. In this case, the water column is well mixed (as is usually during the winter period), with average values around 1028 kg/m^3. This condition will generate *ws* roughly constant and slightly slower sinking than the summer release.

During the summer release the water column is highly stratified as we can see from Fig. 8b. In this case, the particles are initially confined in a surface layer where the density is about 1025 kg/m^3. Under this condition, the settling velocity will be slightly higher than the winter case and the horizontal transport will be more constrained. As they sink, the density rises, and the *ws* decreases, thus allowing for a weaker horizontal transport.

4. Conclusions

The goal of this study was to provide an initial assessment of three-dimensional transport scenarios that may occur when several plastic polymer types reach the marine environment of the GoN. The choice of winter and summer release conditions allowed us to understand the effect of the seasonal hydrodynamic features on particle dynamics.

In the case of particles like PA or PET, the sinking is very rapid, thus the summer and winter scenarios are similar since the horizontal transport and the contribution of the vertical component of the sea are limited. Under these conditions, we may expect a potential particle to settle in areas close to the release zone if we neglect the re-suspension due to turbulent motions. On the other hand, the fate of the particles like PS will depend on the advective features of the horizontal and vertical current field, as well as on the hydrological features of the marine environment.

If we focus on the sea dynamical conditions, the low-intensity surface and sub-surface current fields during the summer period reduce the horizontal particle transport (compared with winter scenarios), thereby enhancing the potential sedimentation in sea areas close to the release zone. In addition, under the dynamical pattern of this period, the particles are displaced not far from the coastline, where the current field is weak.

On the other hand, as a result of the winter mixing of the water column, in that period we observe slightly slower settling rates than in the summer period (according to de la Fuente et al., 2021, see also Fig. 8a and b in Section 3.1). In the latter case, the particles are initially in a surface layer where the density is about 1025 kg/m^3 and, under these conditions, the density difference between the sea field and the plastic polymer is greater than in the winter case, resulting in a higher settling rate. As they sink, the sea density rises, and the settling velocity decreases thus allowing for a weaker horizontal transport.

However, the influence of the vertical component of the sea current field on particle sinking makes the situation more delicate. Through a sensitivity analysis carried out by activating or neglecting w in the vertical particles equation, we highlighted how the re-suspension due to an upward vertical component of the Eulerian current field increases the lifetime of the particles, thus enhancing the horizontal transport contribution and the sedimentation further away from the release zone. This condition occurs, for example, in the summer period, where vertical upward motions due to positive surface divergence fields decrease the particles sinking (especially for PS particles), thus increasing both the residence times and the horizontal transport. In the winter case, on the contrary, although the vertical component works in phase with the settling velocity for the effect of the surface convergence fields, the horizontal transport appears to be greater than in those scenarios where w is not involved in the vertical dynamics. This situation, which certainly needs to be investigated in further detail, could be explained by the fact that, while in the absence of w and under inshore current fields a particle could reach the coastal cell and remains fixed thereafter, the increase of the settling rate that could occur when we take into account *w* may not allow the beaching but yields a transport over greater distances. In other words, the particles are involved in different dynamical regimes that promote their horizontal transport.

In this context, however, it is necessary to emphasize several issues. In our simulations, we have neglected the effect associated with the turbulent nature of the flow field, which could potentially produce different transport scenarios. The turbulent sea motions could enhance or inhibit the sedimentation rate, thereby increasing or reducing the

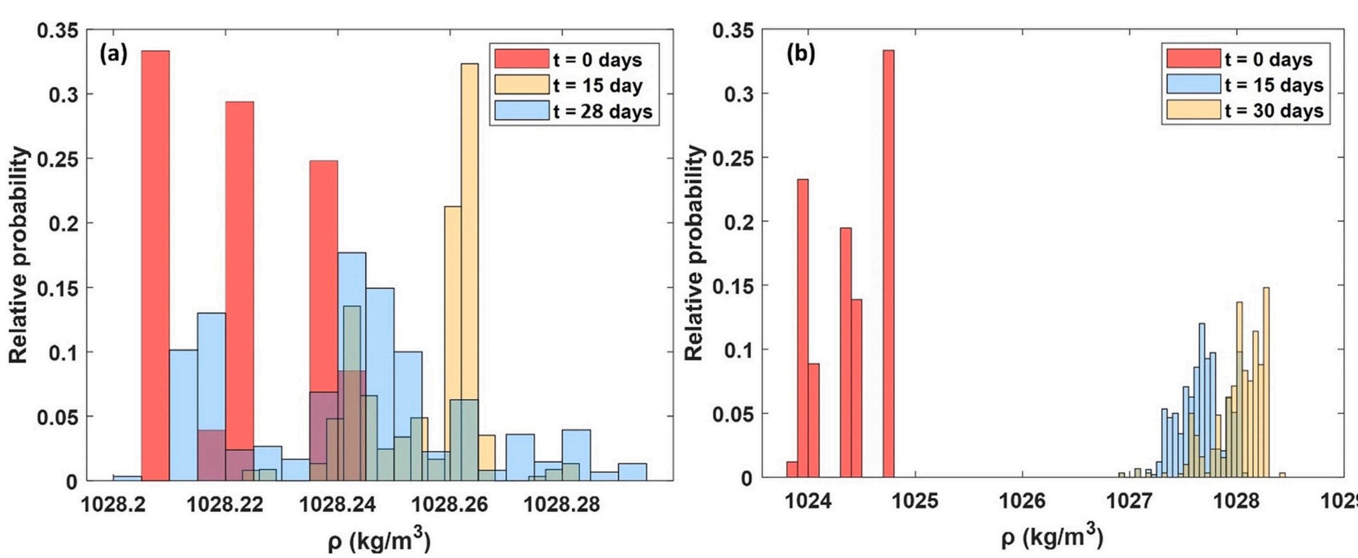

Fig. 8. Normalized probability histogram of the seawater density at the positions of the 1500 PS particles for $t = 0$, 15 and 28 (30) days after the release for February 2016 (a) August 2016 (b) respectively.

particle residence time in the water column (see also Cianelli et al., 2013).

In addition, other physical and biological processes that we have neglected in these simulations, such as the washing-off from the beach, the fragmentation of the plastic polymer types, and the biofouling (Hardesty et al., 2017; Zhang, 2017) may also play a critical role in the particles' evolution.

At the same time, the uncertainty in the release sources, pollutant quantities, and category due to the lack of observed in situ data does not allow to validate our simulations. However, it is worth noting that our aim here was to provide a first attempt at simulating the 3D dynamics in the area, emphasizing the importance of the sub-surface advective field and underlining the importance of monitoring the study area. Indeed, here it is worth highlighting that the building of a careful monitoring network in the GoN could certainly allow us to parameterize these physical and biological processes with a greater degree of detail and realism.

Finally, the use of surface drifters, as well as the deployment of innovative technologies for in-situ observation (such as Unmanned Aerial Vehicles, optical satellite sensors, or the use of ROVs for sea bottom monitoring), would allow us to validate our transport simulations as well as to provide more targeted analyses.

CRediT authorship contribution statement

Methodology, P.d.R., D.C. and S.P.; software, L.G.; model data, P.d.R.; data curation, L.G. and P.d.R.; writing—original draft preparation, L.G.; writing—review and editing, L.G., P.d.R., D.C., S.P. and E.Z.; project administration, E.Z. and S.P. All authors have read and agreed to the published version of the manuscript.

Declaration of competing interest

The authors declare that they have no known competing financial interests or personal relationships that could have appeared to influence the work reported in this paper.

Data availability

The field data and the model outputs are available upon request addressed to the corresponding author.

Acknowledgments

SKIRON/Eta modeling data was provided by G. Kallos and of the National and Kapodistrian University of Athens. This work was partly supported by the 2017 PRIN project EMME (Exploring the fate of Mediterranean microplastic: from distribution pathways to biological effects), funded by the Italian Ministry for Research (grant agreement no. 2017WERYZP).

References

Albanese, S., De Vivo, B., Lima, A., Cicchella, D., Civitillo, D., Cosenza, A., 2010. Geochemical baselines and risk assessment of the Bagnoli brownfield site coastal sea sediments (Naples, Italy). J. Geochem. Explor. 105, 19–33. https://doi.org/10.1016/j.gexplo.2010.01.007.

Andrady, A.L., 2017. The plastic in microplastics: a review. Mar. Pollut. Bull. 119, 12–22. https://doi.org/10.1016/j.marpolbul.2017.01.082.

Angiolillo, M., di Lorenzo, B., Farcomeni, A., Bo, M., Bavestrello, G., Santangelo, G., Cau, A., Mastascusa, V., Cau, A., Sacco, F., et al., 2015. Distribution and assessment of marine debris in the deep Tyrrhenian Sea (NW Mediterranean Sea, Italy). Mar. Pollut. Bull. 92, 149–159. https://doi.org/10.1016/j.marpolbul.2014.12.044.

Baldi, F., Bargagli, R., Focardi, S., Fossi, C., 1983. Mercury and chlorinated hydrocarbons in sediments from the Bay of Naples and adjacent marine areas. Mar. Pollut. Bull. 14, 108–111. https://doi.org/10.1016/0025-326X(83)90311-9.

Beletsky, D., Schwab, D., McCormick, M., 2006. Modeling the 1998–2003 summer circulation and thermal structure in Lake Michigan. J. Geophys. Res. Oceans 111. https://doi.org/10.1029/2005JC003222.

Beletsky, D., Mason, D.M., Schwab, D.J., Rutherford, E.S., Janssen, J., Clapp, D.F., Dettmers, J.M., 2007. Biophysical model of larval yellow perch advection and settlement in Lake Michigan. J. Gt. Lakes Res. 33, 842–866. https://doi.org/10.3394/0380-1330(2007)33[842:BMOLYP]2.0.CO;2.

Berntsen, J., Skagen, D.W., Svendsen, E., 1994. Modelling the transport of particles in the North Sea with reference to Sandeel larvae. Fish. Oceanogr. 3, 81–91. https://doi.org/10.1111/j.1365-2419.1994.tb00051.x.

Blumberg, A.F., Mellor, G.L., 1987. A description of a three-dimensional coastal ocean circulation model. In: Three-Dimensional Coastal Ocean Models. American Geophysical Union (AGU), pp. 1–16 (ISBN 978-1-118-66504-6).

Castagno, P., de Ruggiero, P., Pierini, S., Zambianchi, E., De Alteris, A., De Stefano, M., Budillon, G., 2020. Hydrographic and dynamical characterisation of the Bagnoli-Coroglio Bay (Gulf of Naples, Tyrrhenian Sea). Chem. Ecol. 36, 598–618. https://doi.org/10.1080/02757540.2020.1772244.

Cheng, N.-S., 1997. Simplified settling velocity formula for sediment particle. J. Hydraul. Eng. 123, 149–152. https://doi.org/10.1061/(ASCE)0733-9429(1997)123:2(149).

Cianelli, D., Uttieri, M., Buonocore, B., Falco, P., Zambardino, G., Zambianchi, E., 2012. Dynamics of a very special Mediterranean coastal area: the Gulf of Naples. In: Mediterranean Ecosystems: Dynamics, Management and Conservation, pp. 129–150 (ISBN 978-1-61209-146-4).

Cianelli, D., Uttieri, M., Guida, R., Menna, M., Buonocore, B., Falco, P., Zambardino, G., Zambianchi, E., 2013. Land-based remote sensing of coastal basins: use of an HF radar to investigate surface dynamics and transport processes in the Gulf of Naples. In: Remote Sensing: Techniques, Applications and Technologies, pp. 1–30 (ISBN 978-1-62417-140-6.).

Cooper, D., Corcoran, P., 2010. Effects of mechanical and chemical processes on the degradation of plastic beach debris on the island of Kauai, Hawaii. Mar. Pollut. Bull. https://doi.org/10.1016/j.marpolbul.2009.12.026.

Csanady, G.T., 1980. Turbulent Diffusion in the Environment. D. Reidel Publishing Company, Dordecht, p. 260.

de la Fuente, R., Drótos, G., Hernández-García, E., López, C., van Sebille, E., 2021. Sinking microplastics in the water column: simulations in the Mediterranean sea. Ocean Sci. 17, 431–453. https://doi.org/10.5194/os-17-431-2021.

de Leo, A., Cutroneo, L., Sous, D., Stocchino, A., 2021. Settling velocity of microplastics exposed to wave action. J. Mar. Sci. Eng. 9 (2), 142 (ff10.3390/jmse9020142ff. ffhal-03204185).

Derraik, J.G.B., 2002. The pollution of the marine environment by plastic debris: A review. Mar. Pollut. Bull. 44, 842–852. https://doi.org/10.1016/S0025-326X(02)00220-5.

de Ruggiero, P., Ernesto, N., Iacono, R., Pierini, S., 2016. A high-resolution modelling study of the circulation along the Campania coastal system, with a special focus on the Gulf of Naples. Cont. Shelf Res. 122 https://doi.org/10.1016/j.csr.2016.03.026.

de Ruggiero, P., Esposito, G., Napolitano, E., Iacono, R., Pierini, S., Zambianchi, E., 2020. Modelling the marine circulation of the Campania coastal system (Tyrrhenian Sea) for the year 2016: analysis of the dynamics. J. Mar. Syst. 210, 103388 https://doi.org/10.1016/j.jmarsys.2020.103388.

Duran, R., Rose, K., Romeo, L., Whiting, J., Vielma, J., Bunn, A., Bauer, J., 2018. Simulation of the 2003 Foss Barge - Point Wells oil spill: a comparison between BLOSOM and GNOME oil-spill models. J. Mar. Sci. Eng. 6. https://doi.org/10.3390/jmse6030104.

Engelund, F.; Hansen, E. A Monograph on Sediment Transport in Alluvial Streams. Tech. Univ. Den. (0stervoldgade 10 Cph. K 1967).

Erni-Cassola, G., Zadjelovic, V., Gibson, M.I., Christie-Oleza, J.A., 2019. Distribution of plastic polymer types in the marine environment; a meta-analysis. J. Hazard. Mater. 369, 691–698. https://doi.org/10.1016/j.jhazmat.2019.02.067.

Fossi, M.C., Vlachogianni, T., Galgani, F., Innocenti, F.D., Zampetti, G., Leone, G., 2020. Assessing and mitigating the harmful effects of plastic pollution: the collective multi-stakeholder driven Euro-Mediterranean response. Ocean Coast. Manag. 184, 105005 https://doi.org/10.1016/j.ocecoaman.2019.105005.

Galgani, F., Hanke, G., Maes, T., 2015. Global distribution, composition and abundance of marine litter. In: Bergmann, M., Gutow, L., Klages, M. (Eds.), Marine Anthropogenic Litter. Springer International Publishing, Cham, pp. 29–56 (ISBN 978-3-319-16510-3).

Gifuni, L., de Ruggiero, P., Cianelli, D., Zambianchi, E., Pierini, S., 2022. Hydrology and dynamics in the Gulf of Naples during Spring of 2016: in situ and model data. J. Mar. Sci. Eng. 10, 1776. https://doi.org/10.3390/jmse10111776.

Griggs, G.B., Johnson, S., 1978. Bottom sediment contamination in the Bay of Naples, Italy. Mar. Pollut. Bull. 9, 208–214. https://doi.org/10.1016/0025-326X(78)90294-1.

Hardesty, B.D., Harari, J., Isobe, A., Lebreton, L., Maximenko, N., Potemra, J., van Sebille, E., Vethaak, A.D., Wilcox, C., 2017. Using numerical model simulations to improve the understanding of micro-plastic distribution and pathways in the marine environment. Front. Mar. Sci. 4. https://doi.org/10.3389/fmars.2017.00030.

Hinderstein, L.M., Marr, J.C.A., Martinez, F.A., Dowgiallo, M.J., Puglise, K.A., Pyle, R.L., Zawada, D.G., Appeldoorn, R., 2010. Theme section on "mesophotic coral ecosystems: characterization, ecology, and management". Coral Reefs 29, 247–251. https://doi.org/10.1007/s00338-010-0614-5.

Horton, A.A., Dixon, S.J., 2018. Microplastics: an introduction to environmental transport processes. WIREs Water 5, e1268. https://doi.org/10.1002/wat2.1268.

Jalón-Rojas, I., Wang, X.H., Fredj, E., 2019. A 3D numerical model to track marine plastic debris (TrackMPD): sensitivity of microplastic trajectories and fates to particle dynamical properties and physical processes. Mar. Pollut. Bull. 141, 256–272. https://doi.org/10.1016/j.marpolbul.2019.02.052.

Law, K., Thompson, R., 2014. Oceans. Microplastics in the seas. Science 345, 144–145. https://doi.org/10.1126/science.1254065.

Lermusiaux, P.F.J., et al., 2019. Plastic pollution in the coastal oceans: characterization and modeling. In: OCEANS 2019 MTS/IEEE Seattle. Institute of Electrical and Electronics Engineers, Seattle, WA, pp. 1–10. https://doi.org/10.23919/OCEANS40490.2019.8962786.

Liubartseva, S., Coppini, G., Lecci, R., Clementi, E., 2018. Tracking plastics in the Mediterranean: 2D Lagrangian model. Mar. Pollut. Bull. 129, 151–162. https://doi.org/10.1016/j.marpolbul.2018.02.019.

Madec, G., 2008. NEMO Ocean Engine. Note du Pole de modélisation. Institut Pierre-Simon Laplace (IPSL), France.

Oddo, P., Adani, M., Pinardi, N., Fratianni, C., Tonani, M., Pettenuzzo, D., 2009. A nested Atlantic-Mediterranean Sea general circulation model for operational forecasting. Ocean Sci. https://doi.org/10.5194/os-5-461-2009.

Ribera d'Alcala, M., Modigh, M., Moretti, M., Saggiomo, V., Scardi, M., Spezie, G., Zingone, A., 1989. Una Storia Infinita. Eutrofizzazione Nella Baia Di Napoli. Oebalia 15, 491–501.

Rocha-Santos, T., Duarte, A.C., 2015. A critical overview of the analytical approaches to the occurrence, the fate and the behavior of microplastics in the environment. TrAC Trends Anal. Chem. 65, 47–53. https://doi.org/10.1016/j.trac.2014.10.011.

Schmidt, C., Krauth, T., Wagner, S., 2017. Export of plastic debris by rivers into the sea. Environ. Sci. Technol. 51, 12246–12253. https://doi.org/10.1021/acs.est.7b02368.

SiDiMar, 2005. Risultati e Prospettive Delle Attività Di Monitoraggio Degli Ecosistemi, Realizzate Nell'ambito Della Linea d'azione Nazionale.

Siegel, D.A., Deuser, W.G., 1997. Trajectories of sinking particles in the Sargasso Sea: modeling of statistical funnels above deep-ocean sediment traps. Deep Sea Res. Part Oceanogr. Res. Pap. 44, 1519–1541. https://doi.org/10.1016/S0967-0637(97)00028-9.

Thushari, G.G.N., Senevirathna, J.D.M., 2020. Plastic pollution in the marine environment. Heliyon 6, e04709. https://doi.org/10.1016/j.heliyon.2020.e04709.

Topçu, N., Oztürk, B., 2010. Abundance and composition of solid waste materials on the western part of the Turkish Black Sea seabed. Aquat. Ecosyst. Health Manag. 13, 301–306. https://doi.org/10.1080/14634988.2010.503684.

Tornero, V., Ribera d'Alcalà, M., 2014. Contamination by hazardous substances in the Gulf of Naples and nearby coastal areas: a review of sources, environmental levels and potential impacts in the MSFD perspective. Sci. Total Environ. 466–467, 820–840. https://doi.org/10.1016/j.scitotenv.2013.06.106.

van Sebille, E., Aliani, S., Law, K.L., Maximenko, N., Alsina, J.M., Bagaev, A., Bergmann, M., Chapron, B., Chubarenko, I., Cózar, A., et al., 2020. The physical oceanography of the transport of floating marine debris. Environ. Res. Lett. 15, 023003 https://doi.org/10.1088/1748-9326/ab6d7d.

Watters, D.L., Yoklavich, M.M., Love, M.S., Schroeder, D.M., 2010. Assessing marine debris in deep seafloor habitats off California. Mar. Pollut. Bull. 60, 131–138. https://doi.org/10.1016/j.marpolbul.2009.08.019.

Zambianchi, E., Iermano, I., Suaria, G., Aliani, S., 2014. Marine Litter in the Mediterranean Sea: An Oceanographic Perspective. https://doi.org/10.13140/RG.2.1.2315.3760.

Zambianchi, E., Trani, M., Falco, P., 2017. Lagrangian transport of marine litter in the Mediterranean Sea. Front. Environ. Sci. 5.

Zhang, H., 2017. Transport of microplastics in coastal seas. Estuar. Coast. Shelf Sci. 199, 74–86. https://doi.org/10.1016/j.ecss.2017.09.032.

Zhiyao, S., Tingting, W., Fumin, X., Ruijie, L., 2008. A simple formula for predicting settling velocity of sediment particles. Water Sci. Eng. 1, 37–43. https://doi.org/10.1016/S1674-2370(15)30017-X.

Zingone, A., Dubroca, L., Iudicone, D., Margiotta, F., Corato, F., Ribera d'Alcalà, M., Saggiomo, V., Sarno, D., 2010. Coastal phytoplankton do not rest in winter. Estuar. Coasts 33, 342–361. https://doi.org/10.1007/s12237-009-9157-9.